Light: Science & Applications (2013) 2, e50; doi:10.1038/lsa.2013.6

www.nature.com/lsa

ORIGINAL ARTICLE

New yellow $Ba_{0.93}Eu_{0.07}Al_2O_4$ phosphor for warm-white light-emitting diodes through single-emitting-center conversion

Xufan Li[1,2], John D Budai[3], Feng Liu[1,2], Jane Y Howe[3], Jiahua Zhang[4], Xiao-Jun Wang[5], Zhanjun Gu[6], Chengjun Sun[7], Richard S Meltzer[2] and Zhengwei Pan[1,2]

Phosphor-converted white light-emitting diodes for indoor illumination need to be warm-white (i.e., correlated color temperature <4000 K) with good color rendition (i.e., color rendering index >80). However, no single-phosphor, single-emitting-center-converted white light-emitting diodes can simultaneously satisfy the color temperature and rendition requirements due to the lack of sufficient red spectral component in the phosphors' emission spectrum. Here, we report a new yellow $Ba_{0.93}Eu_{0.07}Al_2O_4$ phosphor that has a new orthorhombic lattice structure and exhibits a broad yellow photoluminescence band with sufficient red spectral component. Warm-white emissions with correlated color temperature <4000 K and color rendering index >80 were readily achieved when combining the $Ba_{0.93}Eu_{0.07}Al_2O_4$ phosphor with a blue light-emitting diode (440–470 nm). This study demonstrates that warm-white light-emitting diodes with high color rendition (i.e., color rendering index >80) can be achieved based on single-phosphor, single-emitting-center conversion.

Light: Science & Applications (2013) **2,** e50; doi:10.1038/lsa.2013.6; published online 18 January 2013

Keywords: luminescence; single-phosphor-conversion; warm-white light-emitting diode; yellow phosphor

INTRODUCTION

White-light sources based on light-emitting diodes (LEDs) have a promising future in general illumination with advantages over conventional lighting sources (e.g., incandescent, fluorescent and high-intensity discharge lamps), because they are energy-saving, compact and rigid, long-lived and environmentally benign.[1–3] The most popular approach for producing commercial white LEDs is based on a single-phosphor, single-emitting-center-conversion model, which is made by coating an InGaN blue LED with a yellow-emitting phosphor. The first as well as the most widely used yellow phosphor is Ce^{3+}-doped $Y_3Al_5O_{12}$ (YAG:Ce), owing to its many favorable properties such as strong absorption of blue light (~420–480 nm), broad emission band in the visible region (500–700 nm), fast luminescence decay time (<100 ns), high external quantum efficiency (QE, ~75% under blue LED excitation), remarkable chemical and thermal stability and easy synthesis.[4] By virtue of these advantages, white LEDs made of a blue LED and a YAG:Ce phosphor are currently the mainstream in the market and are being widely used in not only point light sources, but also wide-illumination equipment, back-lighting of liquid-crystal TVs and high-power automotive headlights.[5]

Despite their wide applications and high luminous efficacy (>100 lm W^{-1}), one deficiency for white LEDs using only YAG:Ce is that they are limited to high correlated color temperature (CCT; usually ~6000 K) and low color rending index (CRI; usually <75), due to the lack of sufficient red spectral component.[4,6,7] The resulting cool, bluish-white light makes such devices undesirable for indoor use. For indoor lighting, the white light should be warm (CCT<4000 K) with sufficient color rendition (CRI>80).[6]

To obtain warm-white LEDs for general illumination, two strategies have generally been adopted to modify the phosphors. One strategy is based on a single-phosphor, multi-emitting-centers-conversion model, in which additional red-emitting centers are introduced into the YAG:Ce lattice (e.g., Pr^{3+}-codoped YAG:Ce^{3+} (Ref. 8) or creating additional sites for Ce^{3+} with red emission *via* incorporating Si^{4+}–N^{3+} into the YAG:Ce^{3+} lattice[9–11]) to compensate the red spectral deficiency of YAG:Ce. The other strategy is based on a multiphosphors-conversion model in which either a red-emitting material (e.g., CdS-based quantum dots[12,13] or a Eu^{2+}-activated nitride[8,14]) is blended with YAG:Ce powder, or a variety of blue (e.g., $BaSiO_2N_2$:Eu^{2+}), green (e.g., $SrSi_2O_2N_2$:Eu^{2+} or β-SiAlON:Eu^{2+}), yellow (e.g., Ca-α-SiAlON:Eu^{2+}) and red (e.g., $Sr_2Si_5N_8$:Eu^{2+} or $CaAlSiN_3$:Eu^{2+}) emitting phosphors are

[1]College of Engineering, University of Georgia, Athens, GA 30602, USA; [2]Department of Physics and Astronomy, University of Georgia, Athens, GA 30602, USA; [3]Materials Science and Technology Division, Oak Ridge National Laboratory, Oak Ridge, TN 37831, USA; [4]State Key Laboratory of Luminescence and Applications, Changchun Institute of Optics, Fine Mechanics and Physics, Chinese Academy of Sciences, Changchun 130033, China; [5]Department of Physics, Georgia Southern University, Statesboro, GA 30460, USA; [6]Key Laboratory for Biomedical Effects of Nanomaterials and Nanosafety, Institute of High Energy Physics, Chinese Academy of Sciences, Beijing 100049, China and [7]X-ray Science Division, Argonne National Laboratory, Argonne, IL 60439, USA.
Correspondence: Professor ZW Pan, College of Engineering & Department of Physics and Astronomy, University of Georgia, Athens, GA 30602, USA.
E-mail: panz@uga.edu
Received 1 April 2012; revised 27 June 2012; accepted 26 August 2012

mixed together.[15,16] Both the multi-emitting-centers model and multi-phosphors model can produce warm-white light with sufficiently high CRI values (80–98); however, the white light generated by these methods generally suffers a poor emitting-color stability, because the different emitting centers or phosphors exhibit different thermal quenching behaviors of luminescence.[10] Moreover, the multiphosphors systems are difficult to make, because the phosphors have to be synthesized separately, the particle sizes of the phosphors have to be matched to one another to avoid agglomeration or sedimentation, and the final phosphor has to be mixed very homogeneously in exact ratios.[9,11] Considering these problems and the advantages of the single-phosphor-converted (with a single emitting center) YAG:Ce LEDs, we believe that a single-phosphor, single-emitting-center-conversion model is the most reliable and economical way to achieve warm-white LEDs. However, no current single phosphor associated with only one emitting center can simultaneously achieve CCT$<$4000 K and CRI$>$80 when combined with a blue LED.

Here, we report a new yellow barium europium aluminate ($Ba_{0.93}Eu_{0.07}Al_2O_4$) phosphor with a single-Eu^{2+}-emitting center that can simultaneously achieve CCT$<$4000 K and CRI$>$80 when singly combined with a blue (440–470 nm) LED.[17] The warm-white light with good color rendition is attributed to the sufficient red component in the broad yellow emission band of $Ba_{0.93}Eu_{0.07}Al_2O_4$. In addition, the $Ba_{0.93}Eu_{0.07}Al_2O_4$ phosphor is a novel compound with a new orthorhombic lattice structure that has not been synthesized and reported before.

MATERIALS AND METHODS

Materials synthesis

The phosphor was synthesized through a carbothermal reduction and vapor-phase deposition method in a strictly controlled tube furnace system (Supplementary Fig. S1). High-purity BaO (99.99%), Eu_2O_3 (99.99%) and Al_2O_3 (99.99%) powders were mixed and ground with graphite powder (99.99%) at a molar ratio of $BaO/Eu_2O_3/Al_2O_3$/graphite $\sim$1 : 0.05 : 0.2 : 10. The functions of the graphite powder are to reduce the oxides and to provide a weakly reducing environment for the formation of divalent europium (Eu^{2+}). Ultrahigh-purity argon was used as the carrier gas and alumina (purity, 99.8%) plates ($2.5\times2.5\times0.5$ cm^3) were used as the substrates for material deposition and growth.

In a typical run, $\sim$1 g source powder was loaded on an alumina boat that was positioned at the center of an alumina tube. An alumina substrate was placed vertically at the downstream region, $\sim$14 cm away from the source materials for product deposition. The alumina tube was then sealed and evacuated to $\sim2\times10^{-3}$ torr before heating. The furnace was then heated to 1450 ℃ to initiate the carbothermal reaction. The vapor-phase reactants thus generated were transported by 80 sccm (standard cubic centimeters per minute) argon carrier gas to the downstream region to feed the growth of the phosphor on the substrate. The pressure during the growth was kept at $\sim$5 torr, and the growth duration was 2 h. At a furnace temperature of 1450 ℃, a temperature profile along the alumina tube was measured using a thermocouple, as shown in Supplementary Fig. S1. The optimum growth temperature for the pure yellow luminescent product is $\sim$1300 ℃.

Characterization methods

The as-synthesized products were initially examined using a Vista Vision optical microscope, with the sample being excited by a 365-nm ultraviolet (UV) lamp. The morphologies were imaged and analyzed using a scanning electron microscope (SEM; FEI Inspect F FEG SEM) and a transmission electron microscope (TEM; Hitachi HF-3300 FEG STEM/TEM). The composition was analyzed using the energy-dispersive X-ray spectroscopes (EDS) in the SEM and TEM, as well as an inductively coupled plasma-mass spectrometer (ICP-MS, VG PlasmQuad 3).[18] For ICP-MS measurements, 1 mg sample was dissolved in 20 ml, 2% HNO_3 solution.

The valence state of Eu ions in the phosphor was measured using X-ray absorption near edge structure spectroscopy on Eu L_3-edge. The measurement was carried out at room temperature using the linear polarized X-ray at the advanced photon source (APS) beamline 20-BM-B.[19] A multi-element Ge detector was used to select the Eu fluorescence for counting.

The crystal structures were examined using both conventional X-ray powder diffraction (XRD; PANalytical X'Pert PRO diffractometer) with Cu $K\alpha_1$ radiation (λ=1.5406 Å) and synchrotron XRD with a monochromatic X-ray beam (λ=0.413 Å) at the APS beamline 11-BM-B. For the synchrotron measurement, the sample were encapsulated inside a narrow capillary tube and irradiated by the monochromatic X-ray beam. The diffraction patterns were fit by JADE diffraction analysis software (Materials Data, Inc., Livermore, CA, USA) to identify the phases and lattice parameters.

The crystal structures were also measured using polychromatic synchrotron X-ray Laue microdiffraction at the APS beamline 34-ID-E.[20–22] The experimental setup is illustrated in Supplementary Fig. S2. At this facility, a pair of curved Kirkpatrick–Baez reflecting mirrors was used to focus an intense synchrotron X-ray beam with a broad energy range ($\sim$6–22 keV) onto individual nanowire with a beam diameter of $\sim$0.5 μm. The wires were mounted on a Cu TEM grid. Scattering of the polychromatic beam generated a Laue diffraction pattern, consisting of many diffraction peaks, each satisfying Bragg's law for a different set of *hkl* crystal planes. The Laue diffraction pattern was collected using a large area CCD detector. A double-crystal Si monochromator was inserted into the incident X-ray beam to obtain absolute lattice parameters. In addition to diffracted beams, optical luminescence was generated locally at the position where the X-ray beam struck the nanowire. By optically imaging the sample with a high-resolution television camera, we were able to observe the generation and propagation of light by particular wires.

The luminescence emission and excitation spectra were measured using a Horiba Jobin Yvon Fluorolog3−2iHR320 spectrofluorometer with a 450 W Xe lamp as the excitation source. The luminescence QE was measured using a quantum yield accessory attached to the spectrofluorometer.

The emission lifetime was measured under 355 nm excitation from a pulsed Nd:YAG laser. The monitored emission wavelength is 580 nm, which was spectrally separated by a monochromator and was detected using a digital oscilloscope connected to a cooled photomultiplier tube. For the temperature-dependent measurements, the sample was mounted on a homemade heating unit consisting of a copper sample holder, a cartridge heater and an Omega temperature controller. The sample holder was first cooled in a quartz cryostat filled with liquid nitrogen to 77 K and then gradually heated to 450 K (the maximum temperature of our heating unit).

The prototype white LEDs were fabricated by placing a small amount of yellow phosphor (scraped from the growth substrate) on a 470 nm blue InGaN chip (we just have 470 nm chips in hand), followed by encapsulating with transparent silicone resin. The CRI and CCT of the white LEDs were measured using an Ocean Optics USB4000 plug-and-play spectrometer. The measurements were conducted at room temperature.

RESULTS AND DISCUSSION

After growth, the surface of the 2.5 cm×2.5 cm substrate was uniformly covered with a thick (~2 mm) layer of fuzzy products that emit bright yellow luminescence when excited by a 365 nm UV lamp (Figure 1a). When the layer was parted using sharp tweezers and observed under an optical microscope, two kinds of morphologies were identified: powder-like product at the bottom region (~1 mm thick) and wire-like product at the top region (~1 mm thick), both emitting the same yellow luminescence under UV excitation (Figure 1b). SEM and TEM observations showed that the powder consists of irregular particles, thin flakes and short whiskers with sizes around 1 μm (Figure 1c and 1d), while the wires are curved and long with diameters of 0.5–2 μm and lengths of 0.1–1 mm (Figure 1e and 1f). EDS composition analyses revealed that both powder and wires are composed of Ba, Al, Eu and O (Figure 1g), and each element is uniformly distributed across the particles or wires, as measured by EDS elemental line scan in TEM (Figure 1h). Quantitative analyses using EDS and ICP-MS showed consistent Ba/Eu/Al atomic ratio, which is ~0.93 : 0.07 : 2. X-ray absorption near edge structure measurement on the Eu L_3-edge (Supplementary Fig. S3) revealed that the Eu ions are in the divalent state, which is consistent with the reducing synthesis environment and the band-shape photoluminescence (PL) emission (refer to Figure 3a; detailed spectral properties will be discussed later) that typically originates from Eu^{2+} ions.[23] Based on the composition and Eu valence states, the chemical formulas of the yellow luminescent product can be written as $Ba_{0.93}Eu_{0.07}Al_2O_4$. This composition is similar to a hexagonal, green-emitting $BaAl_2O_4$:Eu^{2+} phosphor fabricated by a solid-state reaction method;[24–26] however, they emit completely different luminescence colors, suggesting different crystalline environments for the Eu^{2+} emission in the two host lattices.[27]

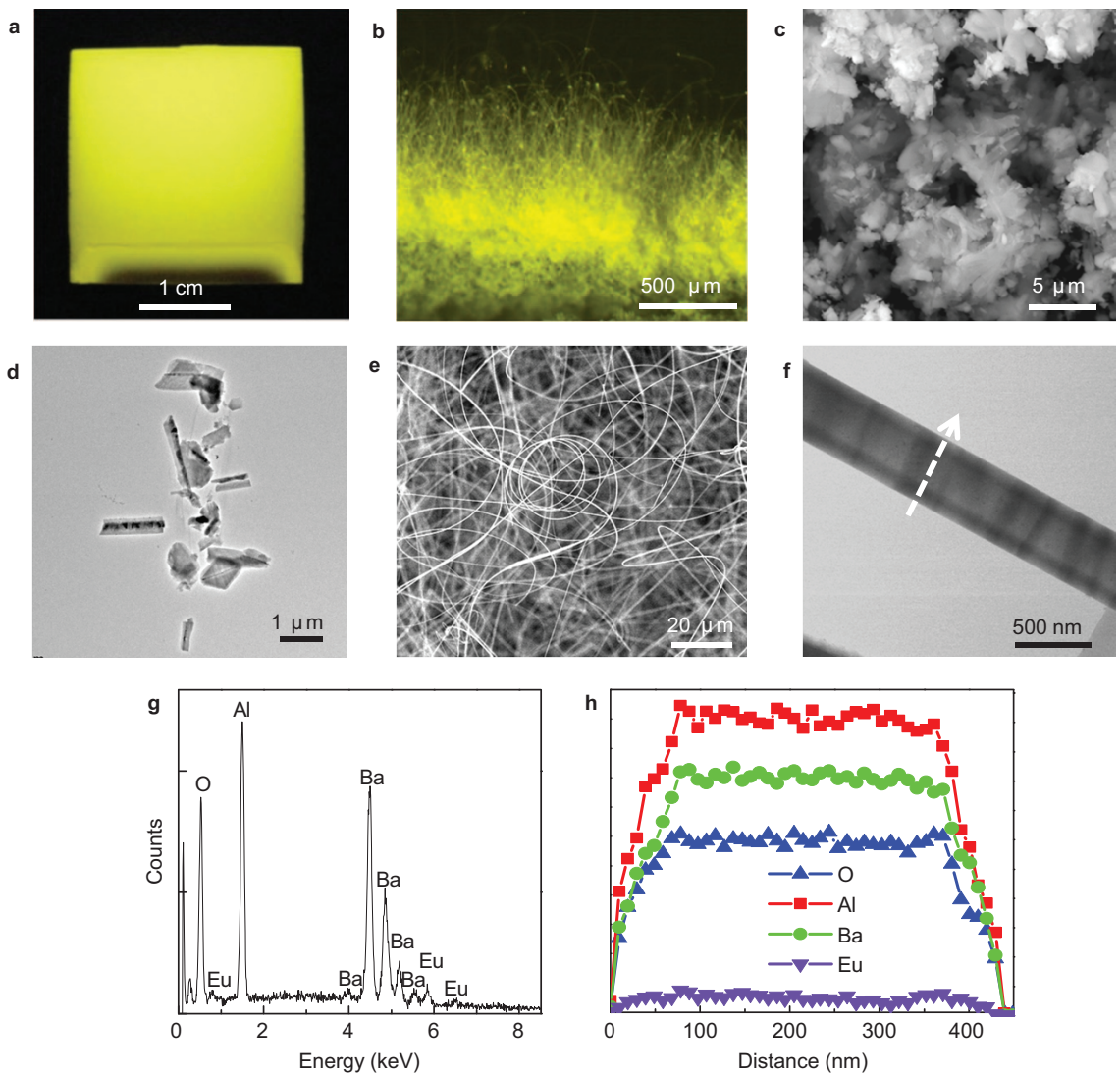

Figure 1 Morphologies and compositions of yellow-emitting nanowires and powders. (**a**) Digital image of yellow luminescent products grown on a 2.5 cm×2.5 cm alumina substrate. The image was taken using a digital camera while the sample was excited by a 365-nm UV lamp. (**b**) Optical microscopy image showing the cross-section of a parted yellow luminescent product layer under the excitation of a 365-nm UV lamp. (**c**) SEM image of powder-like product. (**d**) TEM image of powder-like product. (**e**) SEM image of wire-like product. (**f**) TEM image of an individual wire. (**g**) EDS spectrum of the products acquired in SEM. (**h**) EDS elemental line scan along the radial direction of the wire in (**f**) (the scan direction is indicated by a dashed white arrow). EDS, energy-dispersive X-ray spectroscope; SEM, scanning electron microscope; TEM, transmission electron microscope; UV, ultraviolet.

The crystal structure of the yellow $Ba_{0.93}Eu_{0.07}Al_2O_4$ phosphor was initially characterized using conventional XRD with Cu $K\alpha_1$ radiation (λ=1.5406 Å). The acquired XRD pattern (Supplementary Fig. S4a) is completely different from that of the green $BaAl_2O_4$:Eu^{2+} that is a hexagonal phase (H_{BAO}) with lattice parameters of $a=b$=10.447 Å and c=8.794 Å (JCPDS no. 17–306) (Supplementary Fig. S4b). By searching the ICDD (International Centre for Diffraction Data) database and other commonly available databases such as the Inorganic Crystal Structure Database, we were unable to match the XRD pattern of the yellow luminescent $Ba_{0.93}Eu_{0.07}Al_2O_4$. This means that the $Ba_{0.93}Eu_{0.07}Al_2O_4$ phosphor has a new phase that was not reported before. In order to determine the crystal structure of the yellow $Ba_{0.93}Eu_{0.07}Al_2O_4$ phosphor, we carried out high-resolution synchrotron XRD measurement (λ=0.413 Å; monochromatic energy, 29.9 keV) at the APS beamline 11-BM-B. Figure 2a shows the synchrotron powder XRD pattern of $Ba_{0.93}Eu_{0.07}Al_2O_4$ (The enlarged indexed pattern is given in Supplementary Fig. S5). Analyses using JADE diffraction analysis software (Materials Data, Inc.) show that the $Ba_{0.93}Eu_{0.07}Al_2O_4$ can be best indexed as a new orthorhombic phase (O_{BEAO}) with lattice parameters of a=10.699 Å, b=10.972 Å and c=6.222 Å (The detailed fitting information obtained from Jade analysis is given in Supplementary Fig. S6). It is worth noting that in the synthesis when Eu_2O_3 was excluded from the source and the other synthesis parameters were kept unchanged, only pure $BaAl_2O_4$ with the known H_{BAO} hexagonal phase (JCPDS no. 17–306; Supplementary Fig. S7f), but without luminescence was obtained. Moreover, if the amount of Eu_2O_3 was reduced in the source, the products became a mixture of green $BaAl_2O_4$:Eu^{2+} and yellow $Ba_{0.93}Eu_{0.07}Al_2O_4$ (Supplementary Fig. S7a–d). Interestingly, EDS quantitative analyses on the yellow-emitting wires in the mixture consistently revealed a Ba/Eu/Al molar ratio of ~0.93 : 0.07 : 2 (Supplementary Fig. S8). These results indicate that Eu is indispensable and its concentration is critical for the formation of the new orthorhombic crystal structure. Thus, Eu should be treated as a constituent element of the lattice, rather than a dopant. In this regard, the yellow $Ba_{0.93}Eu_{0.07}Al_2O_4$ phosphor is indeed a new quaternary barium europium aluminate compound.

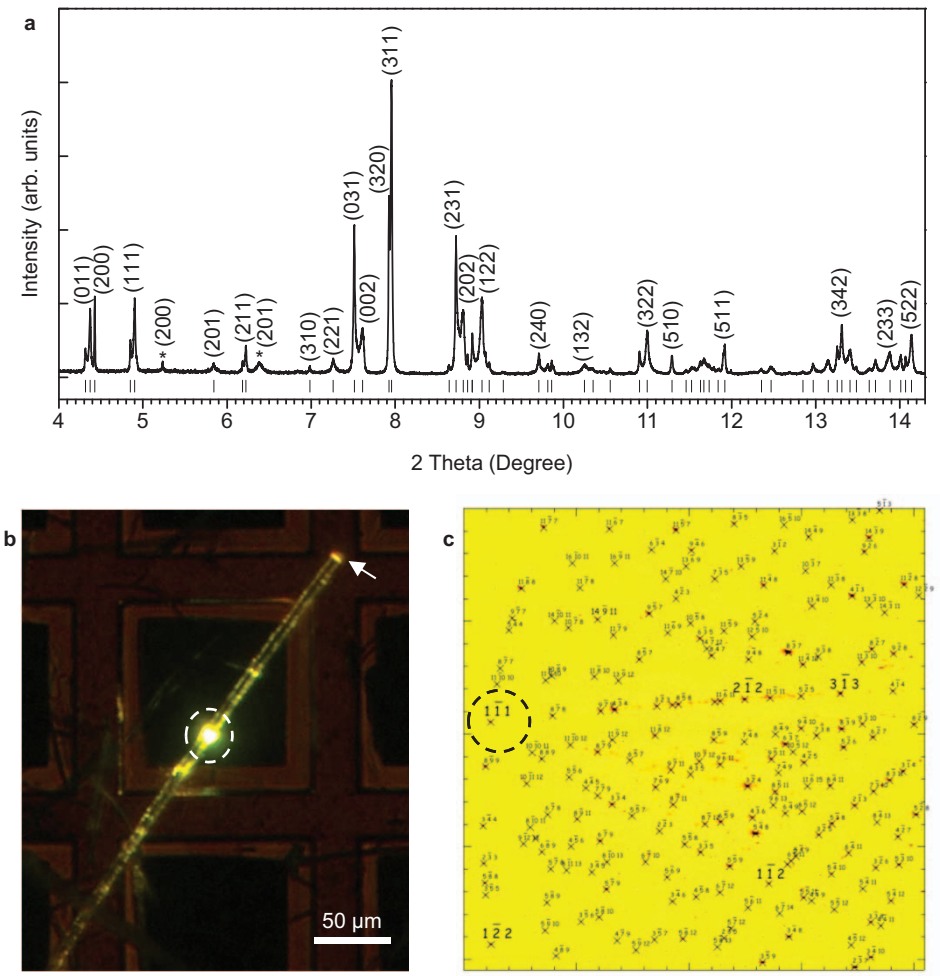

Figure 2 Synchrotron X-ray diffraction measurements of $Ba_{0.93}Eu_{0.07}Al_2O_4$ phosphor. (**a**) Synchrotron powder XRD pattern of yellow $Ba_{0.93}Eu_{0.07}Al_2O_4$ phosphor using a monochromatic radiation (λ=0.413 Å). The tick marks below the pattern indicate the new orthorhombic peak positions identified by JADE software. An enlarged pattern with all peaks indexed is given in Supplementary Fig. S5. The two weak diffraction peaks indicated by * marks belong to the hexagonal $BaAl_2O_4$ (H_{BAO}). More detailed information refers to Supplementary Fig. S5. (**b**) Optical image showing a $Ba_{0.93}Eu_{0.07}Al_2O_4$ wire being struck by a focused polychromatic synchrotron X-ray microbeam (~0.5 μm diameter). The position of the X-ray beam is indicated by a dashed white circle. Yellow luminescence was generated locally, propagated along the wire, and emanated out at wire's end (indicated by a white arrow head). The wire was mounted on a copper TEM grid. (**c**) Indexed Laue microdiffraction pattern acquired from the wire in (**b**) with the orthorhombic (1-11) pole near the surface normal circled. TEM, transmission electron microscope; XRD, X-ray diffraction.

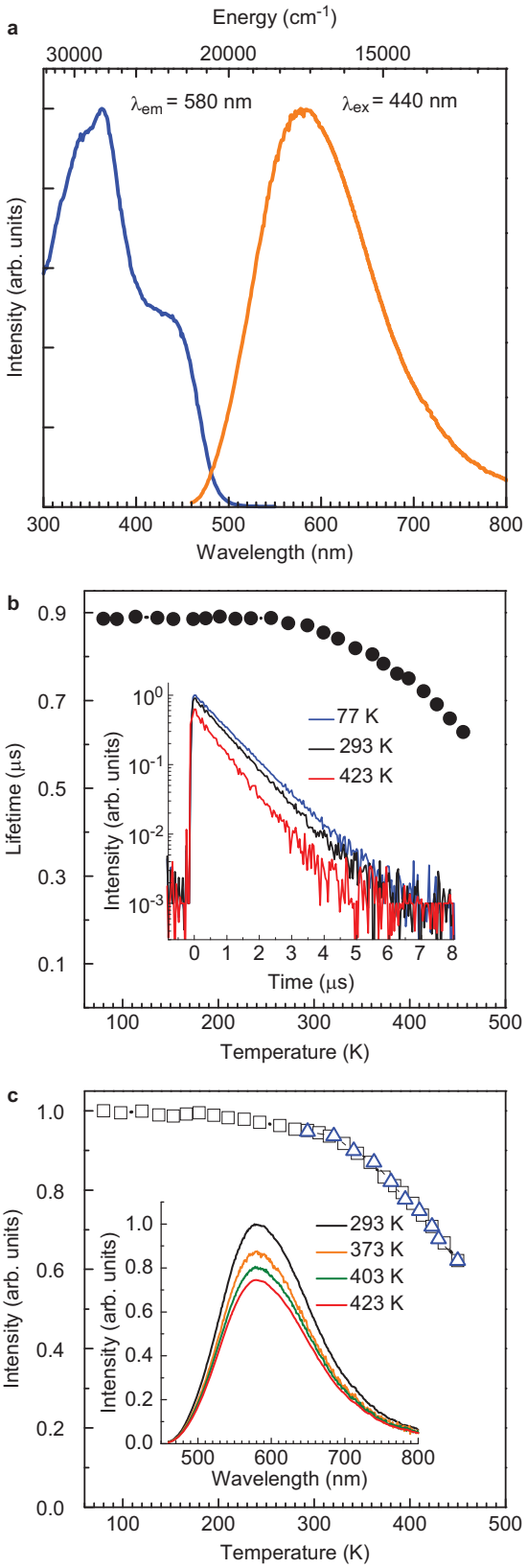

Figure 3 Luminescence properties of $Ba_{0.93}Eu_{0.07}Al_2O_4$ phosphor. (**a**) Normalized luminescence excitation and emission spectra of $Ba_{0.93}Eu_{0.07}Al_2O_4$ phosphor at room temperature. The excitation spectrum (blue curve) was obtained by monitoring 580 nm emission and the emission spectrum (orange curve) was acquired under 440 nm light excitation. (**b**) Temperature dependence of the lifetime of Eu^{2+} emission in $Ba_{0.93}Eu_{0.07}Al_2O_4$ at temperatures from 77 to 450 K. A 355 nm Nd:YAG laser was used as the excitation source and the monitored emission wavelength is 580 nm. Inset is the luminescence decay curves measured at 77, 293 and 423 K. (**c**) Temperature dependence of the integrated emission intensity of $Ba_{0.93}Eu_{0.07}Al_2O_4$ excited by 440 nm light at temperatures from 77 to 450 K. Open squares: data recorded during the heating process from 77 to 450 K. Open blue triangles: data recorded during the cooling process from 450 to 293 K. Inset is the emission spectra at 293, 373, 403 and 423 K.

The structure of the new orthorhombic phase of $Ba_{0.93}Eu_{0.07}Al_2O_4$ was further verified by spatially-resolved polychromatic synchrotron X-ray Laue microdiffraction measurements carried out on individual wires at the APS beamline 34-ID-E. In this approach, a focused synchrotron X-ray beam (~0.5 μm in diameter) with a broad range of energies (~6–22 keV) is incident on individual $Ba_{0.93}Eu_{0.07}Al_2O_4$ wires mounted on a copper TEM grid and excites strong yellow emission (Figure 2b). Scattering of the polychromatic beam generates a Laue diffraction pattern (Figure 2c) that consists of over 150 sharp diffraction peaks, each satisfying Bragg's law for a different set of *hkl* crystal planes. These sharp diffraction peaks reveal good crystal quality of the $Ba_{0.93}Eu_{0.07}Al_2O_4$ wire. All the peaks in the pattern can be well indexed using the new orthorhombic unit cell with lattice parameters of a=10.66 Å, b=10.89 Å and c=6.29 Å, which is in good agreement with the JADE analysis (Figure 2a).

The optical properties of the $Ba_{0.93}Eu_{0.07}Al_2O_4$ phosphor (a mixture of powder and wires) were studied using spectral methods. Figure 3a shows the normalized excitation and emission spectra of $Ba_{0.93}Eu_{0.07}Al_2O_4$ at room temperature. The excitation spectrum monitored at 580 nm emission covers the near-UV and blue regions (from 300 to ~500 nm), containing two bands with the peaks at ~360 and ~440 nm. The emission spectrum is excitation-wavelength-independent; excitation with light at 300–490 nm can consistently produce a very broad single Eu^{2+} emission band that peaks at 580 nm and covers a wide spectral region ranging from blue to deep red. The emission band exhibits a full width at half maximum (FWHM) of ~3767 cm^{-1} and a Stokes Shift of emission of ~6930 cm^{-1} (the Stokes shift was roughly estimated as twice of the energy difference between the peak energy of the emission band and the zero-phonon line energy that was empirically determined as the intersection point of the excitation spectrum and emission spectrum[28]). Both the FWHM and Stokes shift values are much larger than those of the normal Eu^{2+} emissions in solids (the typical FWHM and Stokes shift values are ~1350 and ~1600 cm^{-1}, respectively).[23] This indicates that as far as the FWHM and Stokes shift of emission are concerned, the broadband yellow emission in $Ba_{0.93}Eu_{0.07}Al_2O_4$ is uncharacteristic of the normal Eu^{2+} $4f^65d^1 \rightarrow 4f^7$ emission.

To better understand the luminescence of $Ba_{0.93}Eu_{0.07}Al_2O_4$ phosphor, we measured the temperature-dependent emission lifetimes and emission intensities at 77–450 K, as plotted in Figure 3b and 3c, respectively. The emission lifetimes were determined by measuring and fitting the emission decay curves at different temperatures between 77 and 450 K. The inset of Figure 3b shows three decay curves acquired at 77, 293 and 423 K. All decay curves exhibit single exponential behavior. The emission lifetime at 77–250 K is ~0.9 μs (Figure 3b), which is close to the typical value (~1.1 μs) of the normal Eu^{2+} $4f^65d^1 \rightarrow 4f^7$ emission in solids.[29] The emission lifetime starts to drop at 250 K, accompanied by a decrease of the emission intensity (Figure 3c). At 450 K, the emission lifetime and intensity drop to ~70% and ~60% of their respective values at 77 K. This indicates that the

quenching temperatures (the temperature at which the lifetime or intensity has decreased to half of its initial value at low temperature) for both lifetime and intensity are higher than 450 K, which is characteristic of the normal Eu^{2+} $4f^65d^1 \rightarrow 4f^7$ emission. The emission lifetime shows a higher quenching temperature than the emission intensity, which may be attributed to the increased reabsorption at higher temperature.[30] In addition, the temperature dependence of emission intensity in the cooling process from 450 to 293 K (represented by blue triangles in Figure 3c) is the same as that in the heating process, indicating that the thermal quenching is recoverable without thermal degradation of the phosphor. Finally, even though the emission intensity is temperature dependent, the shape of the emission band of $Ba_{0.93}Eu_{0.07}Al_2O_4$ remains unchanged from 293 to 450 K (inset of Figure 3c), showing a very good emitting-color stability of the phosphor.

The spectral results in Figure 3 show that the $Ba_{0.93}Eu_{0.07}Al_2O_4$ phosphor exhibits both uncharacteristic (i.e., extraordinary large FWHM and Stokes shift of emission) and characteristic (i.e., typical

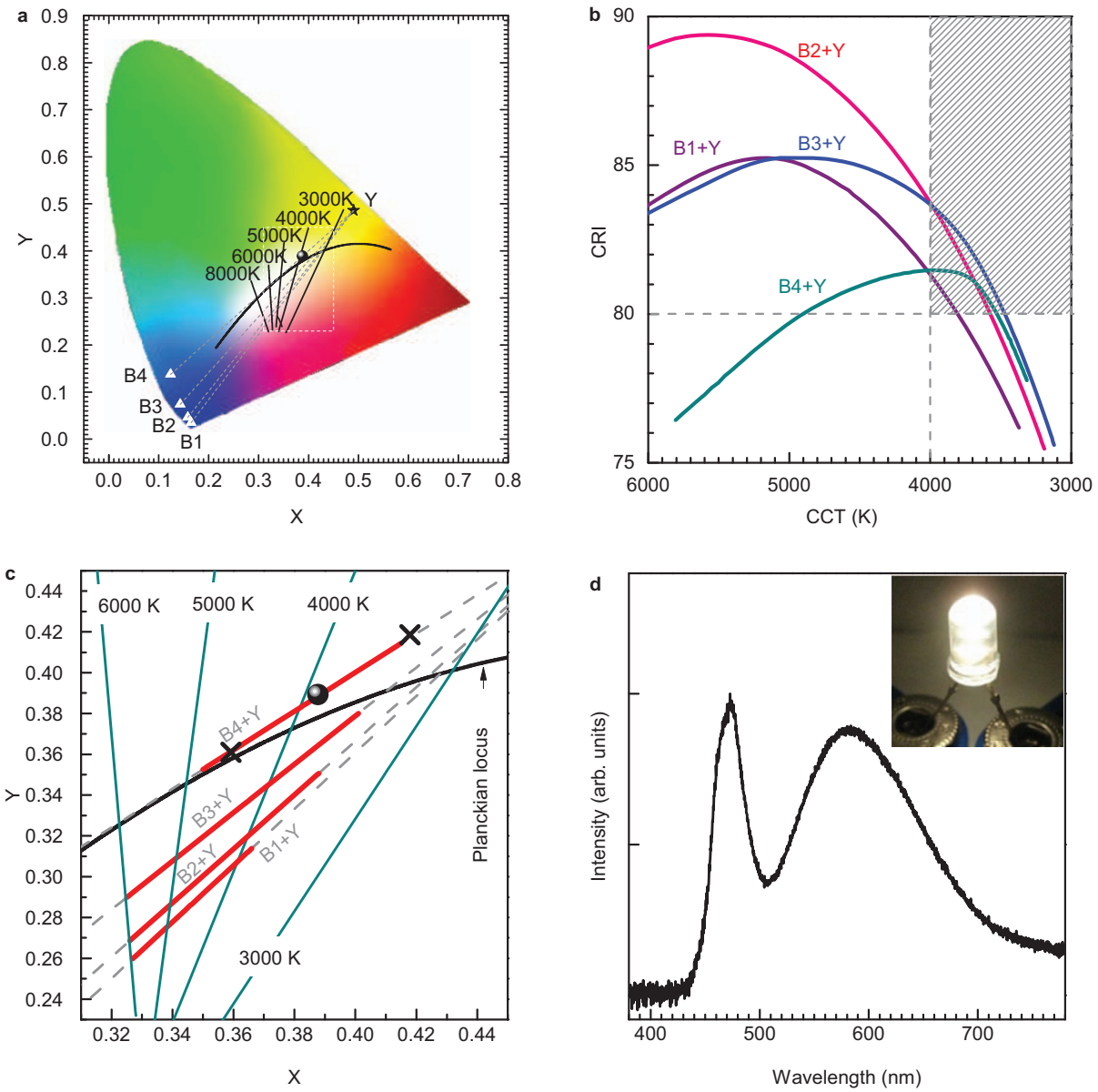

Figure 4 Simulated white emissions and prototype warm-white LED based on $Ba_{0.93}Eu_{0.07}Al_2O_4$ phosphor. (**a**) Chromaticity coordinates on CIE 1931 diagram. The black star, Y, represents the color point of the emission from $Ba_{0.93}Eu_{0.07}Al_2O_4$ phosphor. The four white triangles represent the color points of four blue LEDs emitting at 440 nm (B1), 450 nm (B2), 460 nm (B3) and 470 nm (B4). The black dot represents the color point of the emission from a prototype warm-white LED in (d). The black straight lines are the lines of constant correlated color temperatures from 3000 to 8000 K. The black solid curve is the Planckian locus. (**b**) CRI−CCT diagram of the white emissions simulated by linearly combining the emission spectrum of $Ba_{0.93}Eu_{0.07}Al_2O_4$ with each of the four blue LEDs (B1 to B4). The shaded region confines the area where CCT<4000 K and CRI>80. (**c**) An enlargement of the white boxed region in (**a**) The red lines confine the CCT ranges within which the white emissions have CRI>80. The two black crosses represent the color points of the emission from the two prototype white LEDs in Supplementary Fig. S10. (**d**) Emission spectrum of a prototype warm-white LED made of a 470 nm blue LED and $Ba_{0.93}Eu_{0.07}Al_2O_4$ yellow phosphor. Inset is a digital image of the prototype warm-white LED. CCT, correlated color temperature; CRI, color rending index; LED, light-emitting diode.

radiative lifetime of Eu^{2+} ions and high quenching temperature of luminescence) properties of Eu^{2+} emission in solids. Thus, the yellow emission from $Ba_{0.93}Eu_{0.07}Al_2O_4$ should be ascribed to an extreme case of Eu^{2+} $4f^65d^1 \rightarrow 4f^7$ emission.[31]

The above results reveal that we have synthesized a new yellow $Ba_{0.93}Eu_{0.07}Al_2O_4$ phosphor that emits a very broad single Eu^{2+} emission band with sufficient red component under blue light excitation, and exhibits very good thermal stability and emitting-color stability. These properties, especially the enhanced red emission compared with YAG:Ce (Supplementary Fig. S9), make $Ba_{0.93}Eu_{0.07}Al_2O_4$ a very promising material for achieving warm-white LEDs *via* a single-phosphor, single-emitting-center-conversion model. Indeed, in the CIE 1931 chromaticity diagram shown in Figure 4a, the connection of the color point of $Ba_{0.93}Eu_{0.07}Al_2O_4$ phosphor (Y) with each of the color points of four commercial blue LEDs emitting at 440 nm (B1), 450 nm (B2), 460 nm (B3) and 470 nm (B4) can consistently produce white light (i.e., all connection lines pass through the white emission region). We simulated the white emissions by linearly combining the emission spectrum of $Ba_{0.93}Eu_{0.07}Al_2O_4$ with that of each blue LED, calculated their CCT and CRI values using the reported methods,[32,33] and plotted a CRI−CCT diagram, as shown in Figure 4b. In the enlarged CIE 1931 chromaticity diagram shown in Figure 4c, the ranges of white emissions with CRI>80 for the combinations of $Ba_{0.93}Eu_{0.07}Al_2O_4$ with each of the four blue LEDs are highlighted using bold red lines. It is clear from Figure 4b and 4c that warm-white light with CCT<4000 K and CRI>80 can be readily achieved when appropriate amount of $Ba_{0.93}Eu_{0.07}Al_2O_4$ is singly combined with a blue LED emitting at 440–470 nm. The lowest CCT value with CRI>80 for each combination is 3805 K for B1+Y, 3574 K for B2+Y, 3468 K for B3+Y and 3528 K for B4+Y (Figure 4b). For the B4+Y combination, the highest simulated CRI value (81.5) occurs at CCT=3961 K (the corresponding simulated white emission spectrum is shown in Supplementary Fig. S10a).

To verify the simulation results, we fabricated a series of prototype white LED lamps by encapsulating a 470 nm blue InGaN LED chip with various amounts of $Ba_{0.93}Eu_{0.07}Al_2O_4$ phosphor scraped from the growth substrate. Figure 4d shows the emission spectrum and digital image of a warm-white LED lamp with CCT=3910 K and CRI=82 (two other white LED lamps and their emission spectra are displayed in Supplementary Fig. S11). The corresponding color point of this LED lamp is indicated by a black dot on the chromaticity diagram in Figure 4a and 4c. It is clear that the color point of the real LED lamp lands exactly on the simulated line of the B4+Y combination (the color points of the two lamps in Supplementary Fig. S11, as indicated by the black crosses in Figure 4c, also land on the B4+Y line). To the best of our knowledge, this is the first single-phosphor, single-emitting-center-converted white LED lamp achieving simultaneously CCT<4000 K and CRI>80.

The CRI−CCT diagram (Figure 4b) also reveals that when the $Ba_{0.93}Eu_{0.07}Al_2O_4$ phosphor is singly combined with a blue LED emitting at 440–460 nm (i.e., B1–B3), the CRI values of the resulting white LEDs at CCT in the range of 4000–6000 K can be higher than 85, with the highest CRI value for each combination being 85.3 for B1+Y at ~5183 K, 89.4 for B2+Y at ~5578 K, and 85.3 for B3+Y at ~5020 K (the corresponding emission spectra of the simulated white light are shown in Supplementary Fig. S10b–d). Such remarkable high CRI values once again demonstrate the extraordinary capability of $Ba_{0.93}Eu_{0.07}Al_2O_4$ phosphor in rendering colors and its suitability as a converting phosphor in general illumination.

Despite the significantly improved color rendition of $Ba_{0.93}Eu_{0.07}Al_2O_4$ over YAG:Ce, one major hurdle facing $Ba_{0.93}Eu_{0.07}Al_2O_4$ is its low efficiency. The QE of present $Ba_{0.93}Eu_{0.07}Al_2O_4$ is only ~30% under 440 nm excitation and the luminous efficacy of the warm-white LED prototypes shown in Figure 4d and Supplementary Fig. S11 is only around 20 lm W^{-1}. These parameters must be significantly improved in order for $Ba_{0.93}Eu_{0.07}Al_2O_4$ to become a very competitive candidate for general illumination applications. Several factors are possibly responsible for the low QE of the $Ba_{0.93}Eu_{0.07}Al_2O_4$ phosphor. For example, the extremely large Stokes shift of emission (~6930 cm^{-1}; Figure 3a) can cause more heat loss and thus can lower the QE of the phosphor. In addition, lattice defects that can act as luminescence quenching centers may be introduced into the $Ba_{0.93}Eu_{0.07}Al_2O_4$ powder/whiskers during the growth, which can further lower the QE. Nevertheless, since the material is new, we believe that a better understanding of the underlying luminescence mechanisms and further improvement of the synthesis process may lead to an increase in the QE of the phosphor. Moreover, by using a blue LED chip that is more efficient to the $Ba_{0.93}Eu_{0.07}Al_2O_4$ phosphor (e.g. emitting at 440 nm), the luminous efficacy of the prototype white LEDs can be increased.

CONCLUSIONS

We have synthesized a new yellow $Ba_{0.93}Eu_{0.07}Al_2O_4$ phosphor with a new orthorhombic lattice structure by a carbothermal reduction and vapor-phase deposition method. The $Ba_{0.93}Eu_{0.07}Al_2O_4$ phosphor exhibits a broad yellow emission band with sufficient red component and very good thermal stability and emitting-color stability. Warm-white emissions with correlated color temperature <4000 K and color rendering index >80 were readily achieved when combining the $Ba_{0.93}Eu_{0.07}Al_2O_4$ phosphor with a blue LED. The present work demonstrates, for the first time, that warm-white LEDs with high color rendition can be achieved based on single-phosphor, single-emitting-center-conversion. Moreover, the vapor-phase deposition method described herein is new for phosphor fabrication, which opens a new avenue for the synthesis of new, novel LED phosphors.

ACKNOWLEDGMENTS

ZWP acknowledges funding by the US National Science Foundation (CAREER DMR-0955908). ZJG acknowledges support by the National Basic Research Programs of China (973 program, No. 2012CB932504). JDB was supported by the Materials Sciences and Engineering Division, Office of Basic Energy Sciences (BES), US Department of Energy (DOE). Use of the APS beamline 11-BM-B for synchrotron X-ray powder diffraction and beamline 34-ID-E for polychromatic Laue microdiffraction was supported by the Scientific User Facilities Division of BES, US DOE. Use of the APS beamline 20-BM-B for X-ray absorption near edge structure measurement by CJS was supported by US DOE under Contract no. DE-AC02-06CH11357 with Argonne National Laboratory. The TEM characterization was sponsored by Oak Ridge National Laboratory's Shared Research Equipment (ShaRE) User program, which is sponsored by the Division of Scientific User Facilities of BES, US DOE.

1 Schubert EF, Kim JK. Solid-state light sources getting smart. *Science* 2005; **308**: 1274–1278.
2 Solid-State Lighting Research and Development: Multi-Year Program Plan. Office of Energy Efficiency & Renewable Energy, US Department of Energy [updated May 2011]. Available from: http://apps1.eere.energy.gov/buildings/publications/pdfs/ssl/ssl_mypp2011_web.pdf
3 Pimputkar S, Speck JS, DenBaars SP, Nakamura S. Prospects for LED lighting. *Nature Photon* 2009; **3**: 180–182.
4 Setlur AA. Phosphors for LED-based solid-state lighting. *Electrochem Soc Interface* 2009; **18**: 32–36.
5 Yamamoto H. White LED phosphors: the next step. *Proc SPIE* 2010; **7598**: 759808.

6 Krames MR, Shchekin OB, Mueller-Mach R, Mueller GO, Zhou L *et al*. Status and future of high-power light-emitting diodies for solid-state lighting. *J Disp Techn* 2007; **3**: 160–175.
7 Nakamura S. Present performance of InGaN-based blue/green/yellow LEDs. *Proc SPIE* 1997; **3002**: 26–35.
8 Mueller-Mach R, Mueller GO, Krames MR, Trottier T. High-power phosphor-converted light-emitting diodes based on III-Nitrides. *IEEE J Sel Top Quantum Electron* 2002; **8**: 339–345.
9 Setlur AA, Heward WJ, Hannah ME, Happek U. Incorporation of $Si^{4+}-N^{3-}$ into Ce^{3+}-doped garnets for warm white LED phosphors. *Chem Mater* 2008; **20**: 6277–6283.
10 Liu YF, Zhang X, Hao ZD, Wang XJ, Zhang JH. Generation of broadband emission by incorporating N^{3-} into $Ca_3Sc_2Si_3O_{12}$:Ce^{3+} garnet for high rendering white LEDs. *J Mater Chem* 2011; **21**: 6354–6358.
11 Fiedler T, Fries T, Jermann F, Zachau M, Zwaschka F. Phosphor and light source comprising such a phosphor. US Patent no. 7,267,786 B2, 2007.
12 Shen CY, Li K. High color rendering index WLED based on YAG:Ce phosphor and CdS/ZnS core/shell quantum dots. *Proc SPIE* 2009; **7516**: 751609.
13 Ziegler J, Xu S, Kucur E, Meister F, Batentschuk M *et al*. Silica-coated InP/ZnS nanocrystals as converter material in white LEDs. *Adv Mater* 2008; **20**: 4068–4073.
14 Lin CC, Zheng YS, Chen HY, Ruan CH, Xiao GW *et al*. Improving optical properties of white LED fabricated by a blue LED chip with yellow/red phosphors. *J. Electrochem Soc* 2010; **157**: H900–H903.
15 Mueller-Mach R, Mueller G, Krames MR, Höpper HA, Stadler F *et al*. Highly efficient all-nitride phosphor-converted white light emitting diode. *Phys Stat Sol A* 2005; **202**: 1727–1732.
16 Kimura N, Sakuma K, Hirafune S, Asano K, Hirosaki N *et al*. Extrahigh color rendering white light-emitting diode lamps using oxynitride and nitride phosphors excited by blue light-emitting diode. *Appl Phys Lett* 2007; **90**: 051109.
17 Pan ZW, Liu F, Li XF. Eu^{2+}-activated aluminates nanobelts, whiskers, and powders, methods of making the same and uses thereof. PCT/US Patent no. 11/24268, 2011.
18 Becker JS. Applications of inductively coupled plasma mass spectrometry and laser ablation inductively coupled plasma mass spectrometry in materials science. *Spectrochim Acta B* 2002; **57**: 1805–1820.
19 Heald SM, Brewe DL, Stern EA, Kim KH, Brown FC *et al*. XAFS and micro-XAFS at the PNC-CAT beamlines. *J Synchrotron Rad* 1999; **6**: 347–349.
20 Budai JD, Yang WG, Tamura N, Chung J-S, Tischler JZ *et al*. X-ray microdiffraction study of growth modes and crystallographic tilts in oxide films on metal substrates. *Nature Mater* 2003; **2**: 487–492.
21 Ice GE, Budai JD, Pang WL. The race to X-ray microbeam and nanobeam science. *Science* 2011; **334**: 1234–1239.
22 Pan ZW, Budai JD, Dai ZR, Liu WJ, Paranthaman MP *et al*. Zinc oxide microtowers by vapor phase homoepitaxial regrowth. *Adv Mater* 2009; **21**: 890–896.
23 Dorenbos P. Energy of the first $4f^7 \rightarrow 4f^6 5d$ transition of Eu^{2+} in inorganic compounds. *J Lumin* 2003; **104**: 239–260.
24 Blasse G, Wanmaker WL, ter Vrugt JW. Some new classes of efficient Eu^{2+}-activated phosphors. *J Electrochem Soc* 1968; **115**: 673.
25 Poort SHM, Blokpoel WP, Blasse G. Luminescence of Eu^{2+} in barium and strontium aluminate and gallate. *Chem Mater* 1995; **7**: 1547–1551.
26 Peng MY, Hong GY. Reduction of Eu^{3+} to Eu^{2+} in $BaAl_2O_4$:Eu phosphor prepared in an oxidizing atmosphere and luminescent properties of $BaAl_2O_4$:Eu. *J Lumin* 2007; **127**: 735–740.
27 Rubio J. Doubly-valent rare-earth ions in halide crystals. *J Phys Chem Solids* 1991; **52**: 101–174.
28 Meijerink A, Blasse G. Luminescence properties of Eu^{2+}-activated alkaline earth haloborates. *J Lumin* 1989; **43**: 283–289.
29 Poort SHM, Meyerink A, Blasse G. Lifetime measurements in Eu^{2+}-doped host lattices. *J Phys Chem Solids* 1997; **58**: 1451–1456.
30 Bachmann V, Ronda C, Meijerink A. Temperature quenching of yellow Ce^{3+} luminescence in YAG:Ce. *Chem Mater* 2009; **21**: 2077–2084.
31 Srivastava AM, Comanzo HA, Camardello S, Chaney SB, Aycibin M *et al*. Unusual luminescence of octahedrally coordinated divalent europium ion in $Cs_2M^{2+}P_2O_7$ (M^{2+}=Ca, Sr). *J Lumin* 2009; **129**: 919–925.
32 Schubert EF. Light-emitting diodes. 2nd edn. Cambridge: Cambridge University Press; 2006. pp313–327.
33 McCamy CS. Correlated color temperature as an explicit function of chromaticity coordinates. *Color Res Appl* 1992; **17**: 142–144.

Supplementary Information for this article can be found on *Light: Science & Applications*' website (http://www.nature.com/lsa/).